Likelihood modelling of the Space Geodesy Facility laser ranging sensor for Bayesian filtering

C. Simpson, A. Hunter, S. Vorgul, E. Delande, J. Franco, D. Clark
School of Engineering & Physical Sciences, Heriot-Watt University, Edinburgh, UK
{ccs30, alh31, sv112, E.D.Delande, jf139, D.E.Clark}@hw.ac.uk

J. Rodriguez Perez
NERC-BGS Space Geodesy Facility, Herstmonceux, UK
josrod@nerc.ac.uk

***Abstract*—This work analyzes the data output of laser ranging data collected from the Space Geodesy Facility (Herstmonceux, UK), and proposes a bespoke likelihood function for its processing in the context of Bayesian filtering. It is then illustrated in a single-target Bayesian filter, performing successfully on simulated and real data, under a variety of noise profiles encountered in typical outputs of the sensor.**

I. Introduction

Maintaining an up-to-date catalogue of the near-Earth orbiting objects, including space debris and man-made satellites, has been identified as a key objective of the Space Situational Awareness (SSA) activity, a topic of growing interest, and a challenge whose difficulty is increasing with the growing number of objects populating the near-Earth space [1]. The detection and tracking of orbiting objects is supported by a range of specific ground-based sensing stations for SSA activities, forming an heterogeneous network (radars, telescope, cameras, etc.) from which noisy measurements of different nature are collected by the individual stations. Fusing the information collected from various space sensing assets through a detection and tracking algorithm is an open challenge, that requires some automation in the pre-processing of each data type produced by individual sensors into a coherent probabilistic description of the tracked objects. Casting Satellite Laser Ranging (SLR) data in a Bayesian framework is a necessary step towards this goal.

As part of a coordinated SSA initiative integrating UK and international assets to maintain a common catalogue of orbiting objects, it is important to have accurate probabilistic models of the sensors that integrate it. This type of analysis has been previously carried out for range-only radars [3], Doppler radars [2], and optical sensors [4], [5]. A strategy for using these models in a multi-target tracking scenario has been discussed in [2].

In this paper the output of the range-only laser sensor at the Herstmonceux Space Geodesy Facility (SGF) is analysed in order to design a sensor model for filtering purposes. The sensor model is then exploited for the design of a single-target Bayesian filter, for which implementations based on a Kalman [6] and a particle filter [7] are explored.

This paper is structured as follows. Section II provides a bried description of the Herstmonceux Space Geodesy Facility, and the specifics of the output data. Section III discusses the modelling of the target tracking algorithm, including the bespoke sensor model for the Herstmonceux Space Geodesy Facility, and the design of the resulting single-target Bayesian filter. The tracking algorithm is then tested on simulated and real data in Section IV.

II. The Space Geodesy Facility

The Space Geodesy Facility in Herstmonceux (East Sussex, UK) [8] is a multi-technique geodetic observatory operating an SLR station, an absolute gravimeter and several Global Navigation Satellite System (GNSS) receivers. Along with forty other similar sites around the world, the SGF in Herstmonceux forms part of the International Laser Ranging Service (ILRS) [9]. The SLR technique, used primarily for geodetic purposes, measures the time of flight of short laser pulses as they travel between the observing stations and orbiting satellites equipped with retroreflectors [10], [11]. Satellites routinely tracked by the ILRS network include low Earth orbiters with scientific payloads (e.g. Grace, Jason-3, Swarm), passive geodetic targets (e.g. LAGEOS, LARES), and various GNSS constellations (e.g. GLONASS, BeiDou, GPS). Capable of providing measurements with sub-centimetre accuracy and precision, SLR is one of the four space geodetic techniques contributing to the realisation of the International Terrestrial Reference Frame [12]. Beyond geodetic applications, SLR can also be employed to track uncooperative space debris objects (i.e. no retroreflectors present) [13], [14].

An Nd:Van pulsed laser (1 KHz repetition rate, 10 ps FWHM pulse width, 1.1 mJ/pulse) at the frequency-doubled wavelength of 532 nm is employed at the SGF laser station. The receiver telescope is a 0.5 m Cassegrain reflector equipped with a Single Photon Avalanche Diode (SPAD) detector. The timing measurements are provided by a home built event timer of 1 ps resolution and 5 ps precision. A strictly single-photon tracking policy is followed at SGF for all satellite targets, whereby the energy levels of the returned pulses are controlled and limited to ensure that, on average, only a single photon is contained in each reflected pulse. This ensures that the

978-1-5090-0326-6/16/$31.00 ©2016 IEEE

laser retroreflector arrays carried onboard the satellite targets are sampled in their entirety, with no preferential detections obtained from points closer to the ground station. In order to limit the negative impact of background and dark noise events, the detector is gated shortly earlier (typically 100 ns) than the predicted range to the satellite. This is necessary due to the high sensitivity of the sensor and the present background radiation. The distribution of returns, excluding actual satellite reflections, are adequately described with a negative exponential distribution, as the detection events follow Poisson statistics. The specific characteristics of the distribution of detected pulses from the satellite targets depend on the shape and orientation of the laser retroreflector arrays.

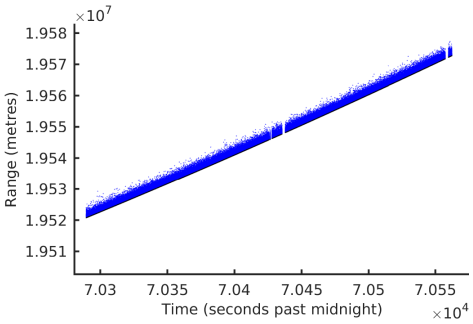

a) Batch 746

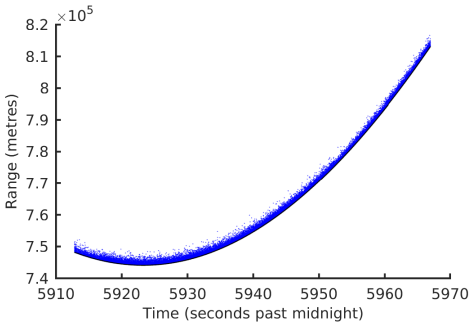

b) Batch 540

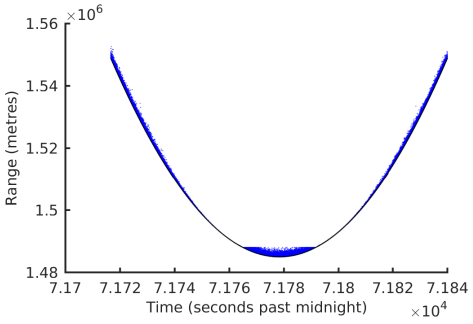

c) Batch 737

Fig. 1: SLR output data. The ground truth is depicted with a black line, the data points are in blue.

Three datasets collected from the SGF laser, named 746, 540, 737 for different satellite passes, were exploited in the context of this paper and are depicted in Fig. 1. These datasets are illustrative of the obtained data. The identities of the observed satellites is known, and the ground truth, shown in Fig. 1 and in subsequent figures, is obtained from an available catalogue. These figures illustrate the typical features of the raw ranging data collected at SGF, though they all present a very noticeable skewness in the data distribution around the ground truth, as explained above and highlighted in the data residuals depicted in Fig. 2. Note in particular the uneven distribution in batch 737 , whose atypical shape in the lower range values is due to a temporal problem in the receiver hardware[1].

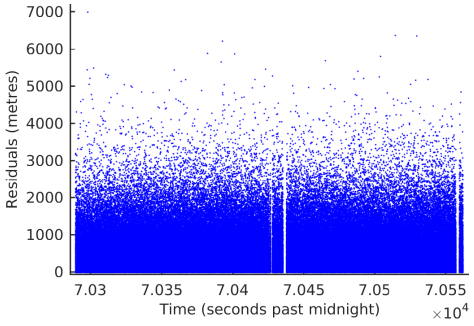

a) Batch 746

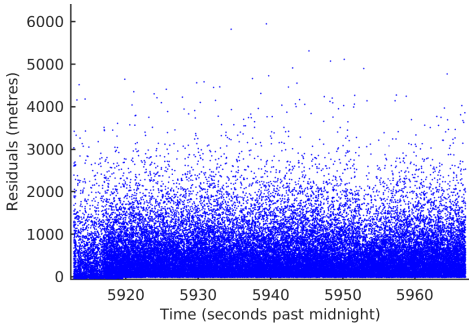

b) Batch 540

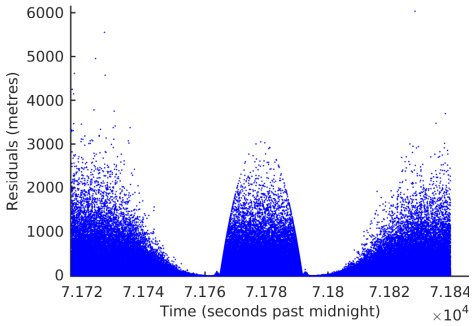

c) Batch 737

Fig. 2: SLR residual data. The data points are in blue.

III. Tracking Algorithm

This section presents the target tracking algorithm proposed in this paper, constructed with the Bayesian estimation framework and designed specifically to process data laser ranging sensors as exploited in the Herstmonceux Space Geodesy Facility.

A. Bayesian estimation: generalities

The state of the target, describing its range r and radial velocity $\dot{r}$ with respect to the sensor, is denoted by the

[1]This is caused by laser overlap, which happens when a pulse is fired at the same time a detector is gated. The pulse backscatters off the atmosphere and triggers the detector. This run was recorded when the overlap avoidance routine was disabled.

vector $x = [r, \dot{r}]' \in \mathcal{X}$, belonging to some target state space $\mathcal{X} \subset \mathbb{R}^2$ covering the admissible values for the target state. In the context of Bayesian filtering, the information on the target state maintained by the operator includes some measure of *uncertainty* associated to the filtered estimate, and is represented by some probability distribution p on the state space $\mathcal{X}$. The time is indexed with some integer k, marking the epochs of data collection.

During the *prediction step* the *predicted distribution* $p_{k|k-1}$, representing the information on the target state at time k prior to the collection of the current observation z_k, is propagated from the output p_{k-1} of the previous time step through the operator's knowledge about the target's dynamic behaviour. During the *updated step* the predicted distribution is corrected to the *posterior distribution* p_k, through the collected observation z_k and the operator's knowledge about the sensor's characteristics (measurement noise, probability of detection, false alarm rate, etc.).

B. Target modelling

Since the target state only depicts the range and radial velocity of the object while passing over the sensor, the target trajectory throughout the observation window is relatively simple and the target motion at time step k is constructed with a simple constant velocity model [15], i.e.

$$x_k = \begin{bmatrix} 1 & \Delta_k \\ 0 & 1 \end{bmatrix} x_{k-1} + n_k, \tag{1}$$

where Δ_k denotes the duration (in unit time) since the last time step $k-1$, $n_k \sim \mathcal{N}(\mathbf{0}, Q_k)$ denotes the process noise, drawn from a Gaussian distribution with zero mean and covariance matrix

$$Q_k = \sigma_k^2 \begin{bmatrix} \frac{\Delta_k^3}{3} & \frac{\Delta_k^2}{2} \\ \frac{\Delta_k^2}{2} & \Delta_k \end{bmatrix}, \tag{2}$$

where the standard deviation σ_k is a model parameter.

C. Sensor modelling

Since the sensor provides data on range only, an observation collected is described by a scalar $z \in \mathcal{Z}$, belonging to some observation space $\mathcal{Z} \subset \mathbb{R}$ covering the admissible values for the observation state.

The peculiar data distribution of the sensor (see Section II) led to the design of a bespoke sensor model for the processing of the Herstmonceux SGF data. Since there is a photon return for every pulse, and the time index of the Bayesian flow coincides with the epochs of data collection (see Section III-A), there is one and only one measurement collected per time step. Due to the reasons discussed in section II, the data distribution has an inverse exponential shape, resulting in the data being skewed in favour of lower ranges (see Fig. 2).

However, little is known about the frequency at which the pulse misses the object of interest, or about the distribution of the background returns and dark noise. For the purpose of filtering, therefore, all the data shall be treated as observations stemming from the object of interest, and the sensor modelling reduces to the design of a suitable likelihood function $\ell(z|x)$, describing the probability that the sensor will return observation z, conditioned on the state x of the object of interest.

Using batch 746 as a training set, an exponential distribution was fitted to the data residuals. The model agreed with the observations well, with a coefficient of determination of $R^2 = 0.9994$. This value is a measure of the correlation between the observed data and the predicted values, and a value so close to one is an indicator that the distribution can be accurately modelled as an exponential distribution. The fitted curve can be seen in Fig. 3, and the obtained equation for the likelihood is

$$\ell(z|x) \propto e^{-2.811.10^{-4}(0.5 \cdot c \cdot z - r)}, \tag{3}$$

where r is the range component of the target state x, in metres, and the observation z is in seconds. The factor $c/2$ is applied to convert from time to distance.

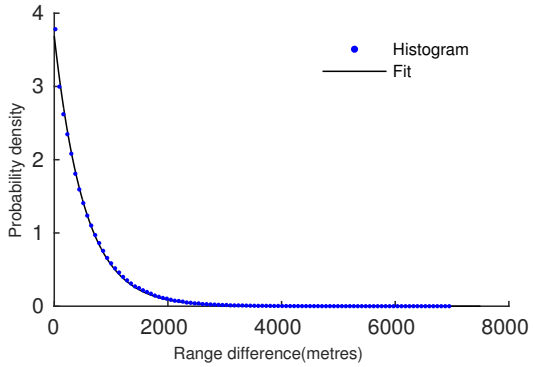

Fig. 3: A histogram of the data residuals of batch 746 using 100 bins, with corresponding exponential fit .

The likelihood function (3) shall be used for the sensor modelling for the remaining of the paper.

D. Filter design

Two approaches have been explored for the design of the filtering solutions: a Kalman filter [6], and a particle filter [7].

1) Kalman filter: The Kalman filter is a well-established filtering solution for single-target detection and tracking problems. Its main advantages lie in the simplicity of its implementation in a practical target tracking algorithm and in the reduced computation cost, though it requires strong modelling assumptions regarding the target motion model and the sensor model [6]. In particular, the Kalman filter assumes that the likelihood function $\ell(\cdot|x)$ follows a Gaussian distribution and is ill-adapted to the representation of heavily-skewed observation profiles such as the one designed for the SGF sensor in Eq. (3).

For the sake of illustration, a Gaussian-distributed likelihood was fit on the data distribution and the resulting Kalman filter was tested on batches 540 and 737. As expected and shown in Fig. 4, the filter assumes a data profile evenly distributed around the true target state and the estimated target trajectory is biased towards higher range values.

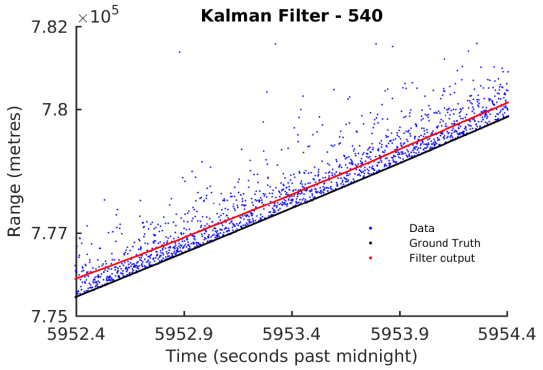

Fig. 4: Kalman filtering applied on batch 540. The ground truth is depicted with a black line, the estimated state with a red line, the data points are in blue.

2) Particle filter: Particle filtering methods impose little restrictions on the nature of the propagated probability distribution p_k, the targets' dynamical behaviour or the sensor observation process; as such, they are widely exploited in tracking problems involving non linear models [7].

In this paper a simple Sequential Importance Resampling (SIR) particle filter is exploited, where the new particles are sampled every time step from the prediction model (1), and reweighted using the likelihood function (3). That is, the posterior probability distribution p_k is approximated by a set of weighted particles $\{x_k^{(i)}, w_k^{(i)}\}_{i=1}^N$, i.e.

$$p_k(x) \simeq \sum_{i=1}^{N} w_k^{(i)} \delta_{x_k^{(i)}}(x), \tag{4}$$

where δ_x is the Dirac delta function centred around x, the number of particles N is a model parameter, and the updated particle set $\{x_k^i, w_k^i\}_{i=1}^N$ is computed from the posterior particle set $\{x_{k-1}^{(i)}, w_{k-1}^{(i)}\}_{i=1}^N$ through the equations

$$\begin{cases} x_k^{(i)} & = \begin{bmatrix} 1 & \Delta_k \\ 0 & 1 \end{bmatrix} x_{k-1}^{(i)} + n_k^{(i)}, \\ w_k^{(i)} & \propto \ell(z_k | x_k^{(i)}) w_{k-1}^{(i)}, \end{cases} \tag{5}$$

where $n_k^{(i)} \sim \mathcal{N}(\mathbf{0}, Q_k)$, $1 \leq i \leq N$. Resampling is done as in the classical bootstrap filter, where a set of particles is sampled from the original weighted set of particles with probability proportional to the original weight. All particles in the resampled set are assigned the same weight. The resulting particle set approximates the same distribution while focusing particles in areas with higher likelihood [16].

IV. Results

In this section, we present the obtained filtering distributions using both simulated data and the Herstmonceux datasets that were previously discussed. Since the Kalman filtering approach yielded biased distributions, we focus on the particle filtering method to present results.

A. Simulated Data

In addition to the data from Herstmonceux, we also simulated our own data where we specified a true trajectory and a noise distribution. This allowed us to test how the filter handles under different realisations. Exponential noise was simulated for 50 Monte Carlo runs, with the following equation:

$$l(x) \propto \begin{cases} e^{-0.0025x}, & x \in [100, 1000], \\ 0, & — \end{cases} . \tag{6}$$

Each Monte Carlo realisation was generated by adding noise sampled from this distribution, and added to the ground truth from dataset 540. The average Root Mean Squared Error (RMSE) can be seen in Fig. 5, alongside error bounds. Here it can be seen how the filter accurately locks into the trajectory after observing the object for a number of time steps.

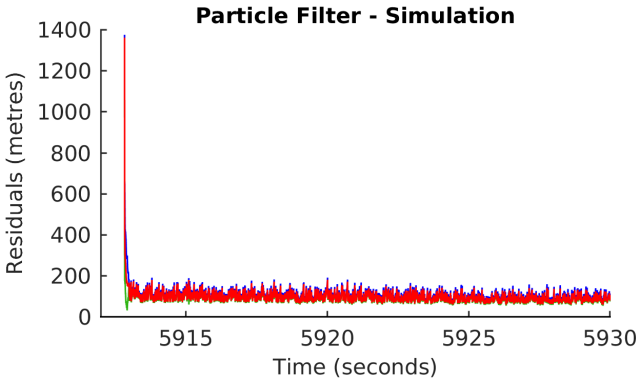

Fig. 5: Average RMSE for 30 simulated Monte Carlo realisations (black line), plus and minus one standard deviation (green and blue lines).

B. Herstmonceux Data

We applied the particle filter to the datasets generated by satellite passes 540 and 737. As it was said before, the training data to fit the exponential likelihood was that of pass 746. The two datasets analysed show different properties. Pass 540 has similar noise properties to the training set, while as it was said before, a temporary hardware issue caused pass 737 to have a more complicated noise structure.

The results of applying the filter on pass 540 can be seen in Fig. 6. It can be seen how the filtering distribution successfully mitigates the measurement noise in spite of the measurements being asymmetrically distributed around the expected range.

Fig. 7 shows the results of applying the filter to pass 737. As it was previously said, a temporary software fault caused the noise distribution to have range-dependent properties. In spite of this noise profile, the filter manages to track the range of the satellite with similar accuracy as in pass 540. In the zoomed-in view, it can be seen how the filtered distribution is robust to sudden changes in noise distribution.

V. Conclusion

We have developed a filtering solution to estimate the range of a satellite from SLR data. The proposed method is capable of handling the noise profiles usually find in SLR problems, which use gated single photon avalanche diodes. The particle filtering framework was exploited, as it allowed us to model the observation likelihood as an exponential

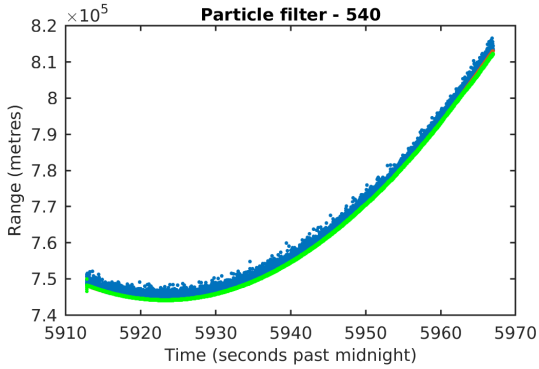

a) Maxima and minima of filtering distribution throughout the estimation (green), and data (blue)

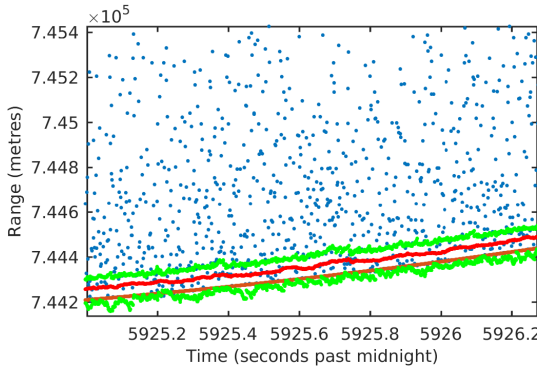

b) Zoomed-in view of the above. Data and extrema as before, ground truth is in orange, and estimate in red.

Fig. 6: Estimation results for pass 540

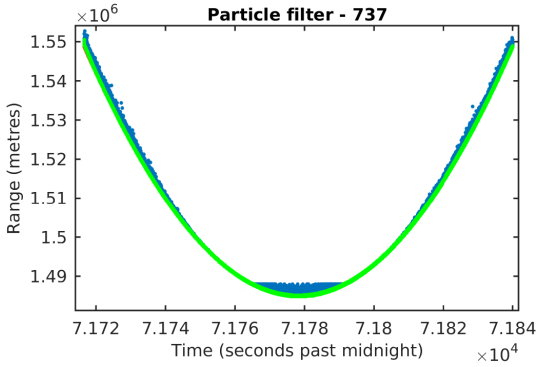

a) Maxima and minima of filtering distribution throughout the estimation (green), and data (blue)

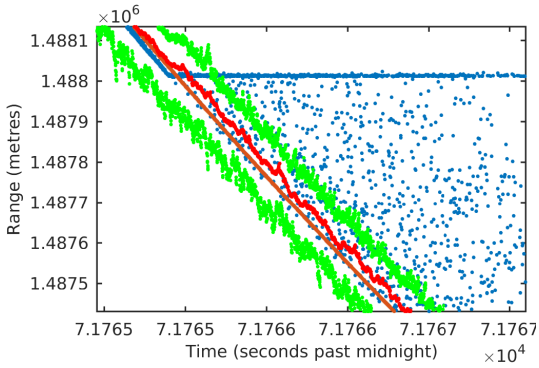

b) Zoomed-in view of the above. Data and extrema as before, ground truth is in orange, and estimate in red.

Fig. 7: Estimation results for pass 737

probability distribution function. The method was tested on both real and simulated data, and its resulting estimates are consistent with the orbital predictions obtained through numerical integration, with the added advantage of providing uncertainty information.

Acknowledgements

This work was supported by the Engineering and Physical Sciences Research Council (EPSRC) Grant number EP/K014277/1 and the MOD University Defence Research Collaboration in Signal Processing.

References

[1] A. Rossi, "The earth orbiting space debris," *Serbian Astronomical Journal*, vol. 170, pp. 1–12, 2005.

[2] E. D. Delande, C. Frueh, J. Houssineau, and D. E. Clark, "Multi-object filtering for space situational awareness," in *2015 AAS/AIAA Spaceflight Mechanics Meeting*, Jan. 2015, pp. AAS 15–406.

[3] A. Pak, D. E. Clark, J. Correa, M. Adams, E. D. Delande, J. Houssineau, J. Franco, and C. Frueh, "Joint Target Detection and Tracking Filter for Chilbolton Advanced Meteoreological Radar Data Processing," in *Advanced Maui Optical and Space Surveillance Technologies Conference*, Sep. 2016, submitted.

[4] O. Hagen, J. Houssineau, I. Schlangen, E. D. Delande, J. Franco, and D. E. Clark, "Joint Estimation of Telescope Drift and Space Object Tracking," in *2016 IEEE Aerospace Conference*, 2016, to appear.

[5] J. Franco, E. D. Delande, C. Frueh, J. Houssineau, and D. E. Clark, "A Spherical Co-ordinate Space Parameterisation for Orbit Estimation," in *IEEE 2016 Aerospace Conference*, 2016, to appear.

[6] R. E. Kalman, "A New Approach to Linear Filtering and Prediction Problems," *Journal of Basic Engineering*, vol. 82, no. 1, pp. 32–45, 1960.

[7] A. Doucet, N. de Freitas, and N. Gordon, *Sequential Monte Carlo Methods in Practice*, ser. Statistics for Engineering and Information Science. Springer, 2001.

[8] SLR Specifications (SGF website, http://sgf.rgo.ac.uk/sysspec/slr.html).

[9] M. Pearlman, J. Degnan, and J. Bosworth, "The international laser ranging service," *Advances in Space Research*, vol. 30, no. 2, pp. 135–143, 2002.

[10] L. Combrinck, "Satellite laser ranging," in *Sciences of Geodesy-I*. Springer, 2010, pp. 301–338.

[11] G. Seeber, *Satellite geodesy: foundations, methods, and applications*. Walter de Gruyter, 2003.

[12] Z. Altamimi, X. Collilieux, and L. Métivier, "Itrf2008: an improved solution of the international terrestrial reference frame," *Journal of Geodesy*, vol. 85, no. 8, pp. 457–473, 2011. [Online]. Available: http://dx.doi.org/10.1007/s00190-011-0444-4

[13] Z.-P. Zhang, F.-M. Yang, H.-F. Zhang, Z.-B. Wu, J.-P. Chen, P. Li, and W.-D. Meng, "The use of laser ranging to measure space debris," *Research in Astronomy and Astrophysics*, vol. 12, no. 2, p. 212, 2012. [Online]. Available: http://stacks.iop.org/1674-4527/12/i=2/a=009

[14] G. Kirchner, F. Koidl, F. Friederich, I. Buske, U. Vlker, and W. Riede, "Laser measurements to space debris from graz {SLR} station," *Advances in Space Research*, vol. 51, no. 1, pp. 21 – 24, 2013. [Online]. Available: http://www.sciencedirect.com/science/article/pii/S0273117712005492

[15] X. Li Rong and V. P. Jilkov, "A Survey of maneuvering Target Tracking. Part I: Dynamic Models," *Aerospace and Electronic Systems, IEEE Transactions on*, vol. 39, no. 4, pp. 1333–1364, Oct. 2003.

[16] N. J. Gordon, D. J. Salmond, and A. F. Smith, "Novel approach to nonlinear/non-gaussian bayesian state estimation," in *IEE Proceedings F (Radar and Signal Processing)*, vol. 140, no. 2. IET, 1993, pp. 107–113.